NACA RM L57C18

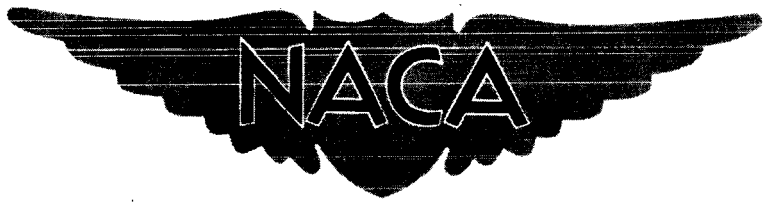

RESEARCH MEMORANDUM

HEAT-TRANSFER AND PRESSURE DISTRIBUTION ON SIX BLUNT NOSES AT A MACH NUMBER OF 2

By Howard S. Carter and Walter E. Bressette

Langley Aeronautical Laboratory
Langley Field, Va.

NATIONAL ADVISORY COMMITTEE
FOR AERONAUTICS

WASHINGTON

April 18, 1957
Declassified January 12, 1961

NATIONAL ADVISORY COMMITTEE FOR AERONAUTICS

RESEARCH MEMORANDUM

HEAT-TRANSFER AND PRESSURE DISTRIBUTION ON SIX BLUNT NOSES AT A MACH NUMBER OF 2

By Howard S. Carter and Walter E. Bressette

SUMMARY

The heat transfer and pressures on the surfaces of six blunt-nose models are presented for angles of attack of 0° and 5°. The tests were made under steady-flow conditions in a free jet at a Mach number of 2 for a Reynolds number per foot of about 14×10^6.

The measured pressure coefficients at an angle of attack of 0° for the hemisphere-cone model agreed very closely with a modified Newtonian theory. On all models transition was encountered because of the effects of surface roughness and corner design. Proper design of the corners of flat-faced models is necessary in order to avoid premature transition downstream. The flat-faced models showed a reduction of heat transfer at the stagnation point of approximately 30 percent below that of the hemisphere-cone model.

INTRODUCTION

The problem of heat alleviation on the nose of a body which is required to enter the atmosphere at high speeds is discussed extensively in reference 1. As indicated in reference 1, one possible solution to the problem of survival of a long-range ballistic missile during atmospheric entry lies in the use of blunt-nose shapes. The blunt-nose shape has high drag which would decelerate the missile prior to its entry into the dense portion of the atmosphere and thus would reduce the heat transfer to the missile surface. Also, the heat-transfer coefficients on a blunt nose are less than those on a pointed nose and more material can be provided to absorb this incoming heat.

Since the publication of reference 1, the National Advisory Committee for Aeronautics has expended considerable effort in an attempt to determine the best external shape for this blunt nose. As was mentioned in

reference 2, a flat nose would be very favorable from the standpoint of both high drag and low heat transfer. Reference 2 further discusses the advantages of the flat nose and presents the results of some exploratory tests for several nose shapes.

A flight-test program on blunt noses using rocket-propelled models at high Mach numbers has been set up by the Langley Pilotless Aircraft Research Division. The tests reported herein were made to obtain preliminary data and to assist in the setting up of this flight-test program. The six blunt-nose models were tested in the preflight jet of the Langley Pilotless Aircraft Research Station at Wallops Island, Va. All tests were made in the 12- by 12-inch preflight jet at sea-level pressure and temperature conditions for a Mach number of 2. The free-stream Reynolds number per foot was approximately 14×10^6 for all tests.

The Mach number of these tests was low in comparison with the Mach numbers for which reentry data are actually needed. Reference 3, however, states that the distribution of the heat transfer on the hemispherical nose is believed to be the same from a Mach number of 2 up to Mach numbers at which dissociation occurs. This relation may also be true for the other nose shapes tested; thus the data in this report may be useful in predicting the heat-transfer distribution on these same shapes at high Mach numbers and hence may influence the designs of the preliminary prototypes.

SYMBOLS

α	angle of attack, deg
c_w	specific heat of skin, Btu/lb-$^\circ$F
C_p	pressure coefficient, $\frac{p_l - p_\infty}{q_\infty}$
ρ_w	mass density of skin, lb/cu ft
h	local aerodynamic heat-transfer coefficient, Btu/sec-sq ft-$^\circ$F
p_l	local static pressure, lb/sq ft
p_∞	free-stream static pressure, lb/sq ft
q_∞	free-stream dynamic pressure, lb/sq ft
S	distance along surface from center line, in.

t	skin thickness, ft
τ	time, sec
T_{aw}	adiabatic wall temperature, $^{\circ}R$
T_t	free-stream stagnation temperature, $^{\circ}R$
T_w	wall temperature, $^{\circ}R$
θ	angle between the model surface and the free-stream direction, deg

APPARATUS

Models

Drawings and photographs of the six models tested are shown in figure 1. The first four models (models A, B, C, and D) differ only in the size of the flat surface at the nose of the model and in the radius of the circular fairing at the corner. Model E is identical in shape to model B except for the 2-inch-radius dimple in the nose, and model F is identical in shape to model D except for a 0.2-inch flat depression on the nose.

All models were made of 1/32-inch-thick Inconel. Because of the spinning process used in construction, the thickness of the skin on the conical portion of the models was considerably reduced below this value. In order to support the thin skin of these models during the tests and also to provide a means of fastening the models to a stand, the interior of the models was filled with balsa and mahogany wood contoured to fit the inside of the models; however, only the balsa made contact with the model skin. Balsa was used for this supporting material since it had the necessary compressible strength to support the surface and also because it had very little mass to act as a heat sink. In order to fasten the model skin to this supporting core, two screws were used at the downstream end of the model in a plane 90° from the measuring plane.

The instrumentation consisted of several iron-constantan thermocouples (no. 30 wire) welded to the interior surface of the skin and several pressure tubes. The thermocouples were all positioned on the surface in a plane passing through the axis of revolution. The first thermocouple on each model was placed in the center of the nose. The pressure tubes were placed in the surface in the same plane as the thermocouples and on the opposite side of the model. In addition, a total-temperature probe was mounted on the stand in a position to measure the

total temperature at the downstream end of the models about $\frac{1}{2}$ inch from the surface.

The surface roughness of the models before the initial test was about 10 microinches. No further polishing was done during the tests.

Test Facility

The investigation reported herein was conducted in the preflight jet test facility located at the Langley Pilotless Aircraft Research Station at Wallops Island, Va. The tests were made in the 12- by 12-inch preflight jet at sea-level pressure and temperature conditions for a free-stream Mach number of 2. This blowdown type of jet is described in reference 4.

A photograph of one of the blunt-nose models mounted at the exit of the 12- by 12-inch nozzle is shown in figure 2. The most forward tip of the model was positioned approximately 1 inch downstream of the nozzle exit. The center line of the model was approximately 0.25 inch below the center line of the nozzle. In this position the model was in a free-stream flow field which was free of any shocks except those originating from the model itself. As shown in the photograph, the model was mounted on a stand which could be rotated to a position placing the model outside of the flow stream. This stand was mounted on a turntable which could be adjusted for angle of attack.

For the tests in which shadowgraphs were made, a shadowgraph camera was mounted on the right-hand side of the nozzle. The spark source used in conjunction with this camera was about 30 feet to the left of the model. Figure 3 shows shadowgraphs of each model made with this camera. In order to show the bow wave, the models have been moved about 1 inch farther downstream for these pictures than they were positioned for the tests. Evidently the only difference in the shock patterns for the two positions was the location of the oblique shocks emanating from the jet exit. In the shadowgraphs, these shocks are shown to be striking near the downstream end of the models. The heat-transfer tests, however, were made 1 inch upstream from the position shown, and only the oblique shock at the top of the picture intercepted the model. The instrumentation, which was in a plane 90° from the plane of the pictures, was free of these oblique shocks.

Another group of oblique shocks parallel to the jet-exit shocks appears a few inches downstream. These downstream oblique shocks were the reflections of the bow wave off the jet boundary. The intersection of the bow wave and jet boundary is shown by the two parallel curved oblique shocks that appear about halfway back on the conical section of

the models. None of these disturbances caused by the bow wave were near the surfaces of the models.

On models C, D, and F, there were oblique shocks immediately downstream of the corners. Apparently, these small-radius corners disturbed the flow considerably more than the large-radius corners on the other models.

TESTS AND PROCEDURE

Range of Variables

Tests were made at a Mach number of 2 for angles of attack of 0° and 5°. The total pressure (115 lb/sq in. absolute) was the same for all tests within 1 percent and did not vary during the tests more than 1 percent. The stagnation temperature of the jet (935° R) varied as much as 2 percent between tests but did not vary more than 1/2 percent during an individual test. The Reynolds numbers varied from zero at the stagnation point of the models to approximately 5×10^6 at the downstream end. The local Reynolds number at each measuring station was based on the distance along the surface from the stagnation point to the station. During the angle-of-attack tests the stagnation point was not on the center line of the model; hence, the distance to each measuring station was changed accordingly.

At the beginning of each test, the model was held out of the jet until the flow became steady; the injector-type stand then swung the model into the jet. It took approximately 1 second for the model to reach the center line of the jet. When the model reached the center line, a microswitch mounted on the arm of the injector stand made contact and the resulting signal was indicated on the recorder. The test then continued at sea-level free-stream conditions for approximately 40 seconds.

Reduction of Data

The aerodynamic heat-transfer coefficients were calculated from data measured during the transient heating of the model at the earliest possible time after the establishment of steady air flow over the model. At this early time, which was 1 second after the model entered the jet, radiation from the model surface and conduction into the backing material as well as along the surface were found to be negligible. If these terms are negligible, the convective heat transferred to the model can be

equated to the heat absorbed by the model skin per unit of time. This relation is expressed in the following approximate equation:

$$h(T_{aw} - T_w) = \rho_w c_w t \frac{dT_w}{d\tau}$$

The aerodynamic heat-transfer coefficient was evaluated by using the mass density ρ_w of the Inconel as 518 lb/cu ft and its specific heat c_w as given in reference 5. The skin thickness t at each thermocouple station was measured before the model was assembled. The thickness varied on the models from about 0.032 inch at the center of the nose to about 0.020 inch at the downstream end. This variation which occurred because of the method of construction was gradual and was assumed to have had no effect on the data reduction. The adiabatic wall temperature at each thermocouple was obtained from theory by assuming isentropic flow around the models.

The skin temperature and its time rate of change were obtained from the measured time histories of the skin temperature. A typical skin temperature and stagnation history is shown in figure 4. This figure shows that, for the early time for which the data are presented, the temperature forcing function $T_{aw} - T_w$ was of large magnitude. Hence, a small error in wall temperature would not affect the heat-transfer coefficient to any great extent. The overall accuracy of the data reduction is believed to be approximately 15 percent.

RESULTS AND DISCUSSION

Figures 5 and 6 as well as table I present the pressure coefficients and heat-transfer coefficients for the six models tested. The heat-transfer curves are presented on a grid in this manner for ease of visualization. The grid is somewhat distorted on the curved portions; hence, the fairing of the data may not be exactly correct in these regions. However, this method was considered best to show the variations in the data between different points on the models. Tests were made at angles of attack of 0° and 5° for models A, B, C, and D, and at an angle of attack of 0° only for models E and F.

Pressure Distributions

Figure 5 shows the pressure distributions for the six models in the form of pressure coefficients. Shown for the conical portion of each model is a theoretical curve for the pressure coefficients at an angle

of attack of 0°. The cone theory (ref. 6) assumes that the cone is pointed and not blunted as in these tests. Also shown for each model is a Newtonian theory curve for an angle of attack of 0° modified as suggested in reference 7. This modification consisted of changing the Newtonian equation to the following equation:

$$C_p = C_{p,max} \sin^2\theta$$

in which $C_{p,max}$ is the pressure coefficient at the stagnation point. Very good agreement was obtained only for model A.

The pressure coefficient on all models with flat noses decreased slightly near the outer edge of the flat section. Model E which had a dimple in the center of the nose showed this same tendency. The modified Newtonian theory had predicted a constant pressure on the flat faces of these models. Reference 7 showed this same decrease of pressure near the outer edge of a flat-faced cylinder.

The effect of an angle of attack of 5° on pressure coefficient is shown to be small on all models except model D. On the leeward side of this model, the small corner radius apparently caused a considerable reduction of the immediate downstream pressure.

Heat-Transfer Coefficients

Effect of roughness.- No effort was made to vary the roughness of the models during these tests; however, the roughness was expected to vary because of the presence of the fine particles of rust and scale which are known to exist in the tunnel airstream. In an attempt to keep the variation of roughness to a minimum, the models were injected into the airstream after the transient starting conditions of the tunnel. Roughness measurements made on the models after the tests showed a significant increase in roughness. Even though all six models reported herein were subject to this change of roughness during the tests, it did not seem to affect them all alike. Models A and B (fig. 6), the models with the greatest corner radius, seemed to have been affected more from this variation in roughness than did models C and D. It seems reasonable to expect that the 0° angle-of-attack data of figure 6 should be either the same or between the values obtained at an angle of attack of 5°. This was the case for models C and D. However, the first test which was made on model A at an angle of attack of 5° with the heat-transfer data taken on the leeward surface and on model B at an angle of attack of 0° (fig. 6) shows that the heat-transfer coefficient is low over the major portion of these models. The other two tests for each model show the heat-transfer coefficient to be considerably higher, perhaps because of the increasing roughness. Table I gives the sequence of these angle-of-attack tests for the models.

Effect of angle of attack.- When the angle of attack was varied on models A and B, it was expected that the local values of heat-transfer coefficient at an angle of attack of 0° would be either the same or between the values obtained for the windward and leeward surfaces at an angle of attack of 5°. However, as previously explained in the subsection on roughness, this was not the case. Hence, for these two models it is felt that the effect of angle of attack on heat transfer cannot be determined from these tests.

The data for models C and D were somewhat as expected and perhaps a rough estimate of the effect of angle of attack can be obtained for these models. As shown in the shadowgraph pictures in figure 3, there were shock waves emanating from the surface just downstream of the corners of these two models. Evidently, changing the angle of attack by 5° changed the position of these shock waves slightly and hence changed the heat-transfer coefficients as shown in figure 6. This effect of an angle-of-attack change of 5° was large at some measuring stations downstream of the corner with only slight differences existing on the flat front face. Another point of interest shown in figure 6 is that the variation in the heat-transfer coefficient between the leeward and windward surfaces at an angle of attack of 5° on the flat face for models C and D is completely reversed downstream of the corners. Apparently, the main effect of this 5° change in angle of attack was to move the transition point farther downstream for the leeward side than for the windward side.

The laminar and turbulent theories shown for the conical portion of each model are Van Driest's flat-plate theories obtained from references 8 and 9, respectively, and modified to three-dimensional flow according to reference 10. The laminar theory shown for the front portion of the models back to the junction with the conical surface is a combination of two theories. A stagnation point theory by Reshotko and Cohen (ref. 11) gave the actual values of heat transfer at the stagnation point and a theory for blunt bodies by Lester Lees (ref. 12) gave the ratios of the heat transfer at the stagnation point to the other points. These two theories are based on the velocity gradients along the surface. Hence, an accurate pressure distribution along the surface is necessary in order to predict the heat transfer. The pressure distribution obtained on models E and F was not sufficient to allow a good fairing. Also, a theory which could predict accurately the pressure distribution on these two models could not be found. Hence, no heat-transfer theory is shown for the front portion of these two models.

Effect of shape.- As previously stated, the primary purpose of these tests was to compare the heat transfer on these models of different shape. Therefore, the heat transfer for all six models is presented compositely in figure 6 for ease of comparison. The fine grid is omitted but the accurate values of the data are given in table II.

When the heat-transfer coefficients for an angle of attack of 0° are compared at the stagnation points on the six models, it can be seen in conjunction with table I that model A has a value of 0.041, model E has a value of 0.038, and the flat-faced models have values that average about 0.029. The flat-faced models show a reduction of the heat-transfer coefficient at the stagnation points of approximately 30 percent below that of the hemisphere-faced model.

The data on the flat-faced models show that the heat-transfer coefficient increases with distance from the stagnation point. This increase in heat-transfer coefficient with increased distance from the stagnation point is also predicted by the theory.

By comparing models B and E, it can be seen that the dimple in the nose of model E was a disadvantage with respect to the heat-transfer coefficient. This was not expected since it was anticipated that a dimple such as this might cause the bow wave in front of the model to be flatter and hence reduce the vorticity present in the flow downstream of the bow wave. The shadowgraphs shown in figure 3 as well as the data indicate that this flattening effect that was anticipated did not occur.

Visual inspection of the shadowgraphs presented in figure 3 indicates that models A and B did not have any shocks in the close vicinity of the models to disturb the flow. Since there were no shocks to trip the boundary layer and cause transition, it appears possible to obtain laminar flow over most of these models if they could be maintained as smooth as they were for the first tests. As shown in the shadowgraphs of figure 3, models C, D, and F had shocks in the close vicinity of the models just downstream of the corners. By comparing the location of these shocks as seen in the shadowgraphs and the heat-transfer data in figure 6, it could very well be concluded that these shocks were the cause of the flow on each of these models changing from laminar to turbulent.

When the six models are compared on the basis of heat-transfer coefficient, it seems that models C, D, and F are undesirable at the Mach number of 2 since shock waves emanating from their surfaces caused turbulent flow on the conical portion. If models A, B, and E are compared, of the three models, model B has the lowest heat-transfer coefficient at the stagnation point. At an angle of attack of 0°, the value of the heat-transfer coefficient for model B at all points is less than that for model E. Also model B seemed to be less affected by roughness than model A was. It appears from these tests therefore that model B, of the six models tested, would be the best.

CONCLUSIONS

From an experimental investigation in a Mach number 2 free jet to determine the heat transfer on the surfaces of six blunt-nose models, the following conclusions can be made:

1. The measured pressure coefficients at an angle of attack of 0° for the hemisphere-cone model agreed very closely with a modified Newtonian theory. The pressure coefficients at an angle of attack of 0° for the other models disagreed considerably with this theory.

2. The flat-faced models showed a reduction of heat-transfer coefficient at the stagnation point of approximately 30 percent below that of the hemisphere-cone model.

3. Proper design of the corners at the edges of flat-faced models is important to avoid premature transition downstream.

4. Transition was encountered on all models because of the effects of surface roughness and corner design.

Langley Aeronautical Laboratory,
National Advisory Committee for Aeronautics,
Langley Field, Va., March 6, 1957.

REFERENCES

1. Allen, H. Julian, and Eggers, A. J., Jr.: A Study of the Motion and Aerodynamic Heating of Missiles Entering the Earth's Atmosphere at High Supersonic Speeds. NACA RM A53D28, 1953.

2. Purser, Paul E., and Hopko, Russell N.: Exploratory Materials and Missile-Nose-Shape Tests in a 4,000° F Supersonic Air Jet. NACA RM L56J09, 1956.

3. Stine, Howard A., and Wanlass, Kent: Theoretical and Experimental Investigation of Aerodynamic-Heating and Isothermal Heat-Transfer Parameters on a Hemispherical Nose With Laminar Boundary Layer at Supersonic Mach Numbers. NACA TN 3344, 1954.

4. Faget, Maxime A., Watson, Raymond S., and Bartlett, Walter A., Jr.: Free-Jet Tests of a 6.5-Inch-Diameter Ram-Jet Engine at Mach Numbers of 1.81 and 2.00. NACA RM L50L06, 1951.

5. Lucks, C. F., Bing, G. F., Matolich, J., Deem, H. W., and Thompson, H. B.: The Experimental Measurement of Thermal Conductivities, Specific Heats, and Densities of Metallic, Transparent, and Protective Materials - Part II. AF Tech. Rep. No. 6145 (Contract No. AF 33(038)-20558), Battelle Memorial Inst., July 1952.

6. Ames Research Staff: Equations, Tables, and Charts for Compressible Flow. NACA Rep. 1135, 1953. (Supersedes NACA TN 1428.)

7. Oliver, Robert E.: An Experimental Investigation of Flow Over Simple Blunt Bodies at a Nominal Mach Number of 5.8. GALCIT Memo. No. 26 (Contract No. DA-04-495-Ord-19), June 1, 1955.

8. Van Driest, E. R.: Investigation of Laminar Boundary Layer in Compressible Fluids Using the Crocco Method. NACA TN 2597, 1952.

9. Lee, Dorothy B., and Faget, Maxime A.: Charts Adapted From Van Driest's Turbulent Flat-Plate Theory for Determining Values of Turbulent Aerodynamic Friction and Heat-Transfer Coefficients. NACA TN 3811, 1956.

10. Van Driest, E. R.: The Problem of Aerodynamic Heating. Aero Eng. Rev., vol. 15, no. 10, Oct. 1956, pp. 26-41.

11. Reshotko, Eli, and Cohen, Clarence B.: Heat Transfer at the Forward Stagnation Point of Blunt Bodies. NACA TN 3513, 1955.

12. Lees, Lester: Laminar Heat Transfer Over Blunt-Nosed Bodies at Hypersonic Flight Speeds. Jet Propulsion, vol 26, No. 4, Apr. 1956, pp. 259-269.

TABLE I.- SEQUENCE OF TESTS

Test	Model	α, deg	Surface
1	A	5	Leeward
2	A	5	Windward
3	A	0	--------
4	B	0	--------
5	B	5	Leeward
6	B	5	Windward
7	C	5	Windward
8	C	5	Leeward
9	C	0	--------
10	D	0	--------
11	D	5	Leeward
12	D	5	Windward
13	E	0	--------
14	F	0	--------

TABLE II.- SUMMARY OF HEAT-TRANSFER DATA

$\alpha = 0^\circ$			$\alpha = 5^\circ$			
			Windward surface		Leeward surface	
Distance, S, in.	C_p	h	C_p	h	C_p	h
Model A						
0		0.041		0.040		0.042
.44		.044		.041		.039
.88	1.480	.067	1.560	.058	1.350	.039
1.32						.036
1.76	.987	.106	1.120	.084	.829	.030
2.20		.085		.092		.029
2.64	.551	.073	.488	.082	.212	.026
3.30	.070		.184	.062	-.038	.018
3.80	.117	.060	.244	.068	-.002	.038
4.30	.123	.065	.249	.062	.010	.061
5.30	.084	.057	.186	.065	.051	.052
Model B						
0		.028		.034		.025
.56	1.620	.028	1.670	.032	1.500	.025
1.12	1.520	.038	1.600	.041	1.440	.038
1.78	.835		.973	.056	.723	.068
2.36	.062	.021	.189	.052	.056	.036
2.86	.058	.022	.190	.074	.071	.035
3.36	.119	.024	.276	.062	-.016	.036
4.36	.120	.037	.266	.063	0	.033
5.36	.120	.044	.252	.060	.075	.054
Model C						
0		.031		.024		.033
.75	1.610	.028	1.640	.023	1.580	.026
1.50	1.430	.038	1.530	.030	1.370	.042
2.30	.130	.015	-.030	.020	-.211	.012
2.80	0	.014	.172	.030	-.118	.009
3.30	.074	.045	.238	.078	-.064	.015
3.80	.122	.059	.318	.064	-.020	.051
4.80	.137	.045	.288	.055	.039	.058
5.80	.162		.303		.121	
Model D						
0		.029		.028		.031
.87	1.600	.029	1.630	.028	1.580	.030
1.75	1.300	.048	1.370	.037	1.250	.061
1.95	.574	.038	.705	.027	.475	.044
2.15	.273	.010	.225	.015	-.304	.010
2.65	.138	.044	.029	.064	-.255	.015
3.15	.018	.058	.199	.081	-.122	.041
3.65	.101	.072	.274	.081	.054	.049
4.65	.122	.054	.270	.071	.011	.050
5.65	.103	.056	.236	.065	.049	.056
Model E						
0		.038				
.70	1.640	.035				
1.20	1.480	.045				
1.70	.940	.040				
2.45	-.001	.038				
2.95	.048	.054				
3.45	.143	.053				
4.45	.076					
5.45	.093	.045				
Model F						
0		.028				
.81	1.630	.024				
1.60	1.580	.044				
1.95	.298	.047				
2.25	-.306	.017				
2.75	-.106	.008				
3.25	.045	.070				
3.75	.138	.071				
4.75	.169	.064				
5.75	.147	.037				

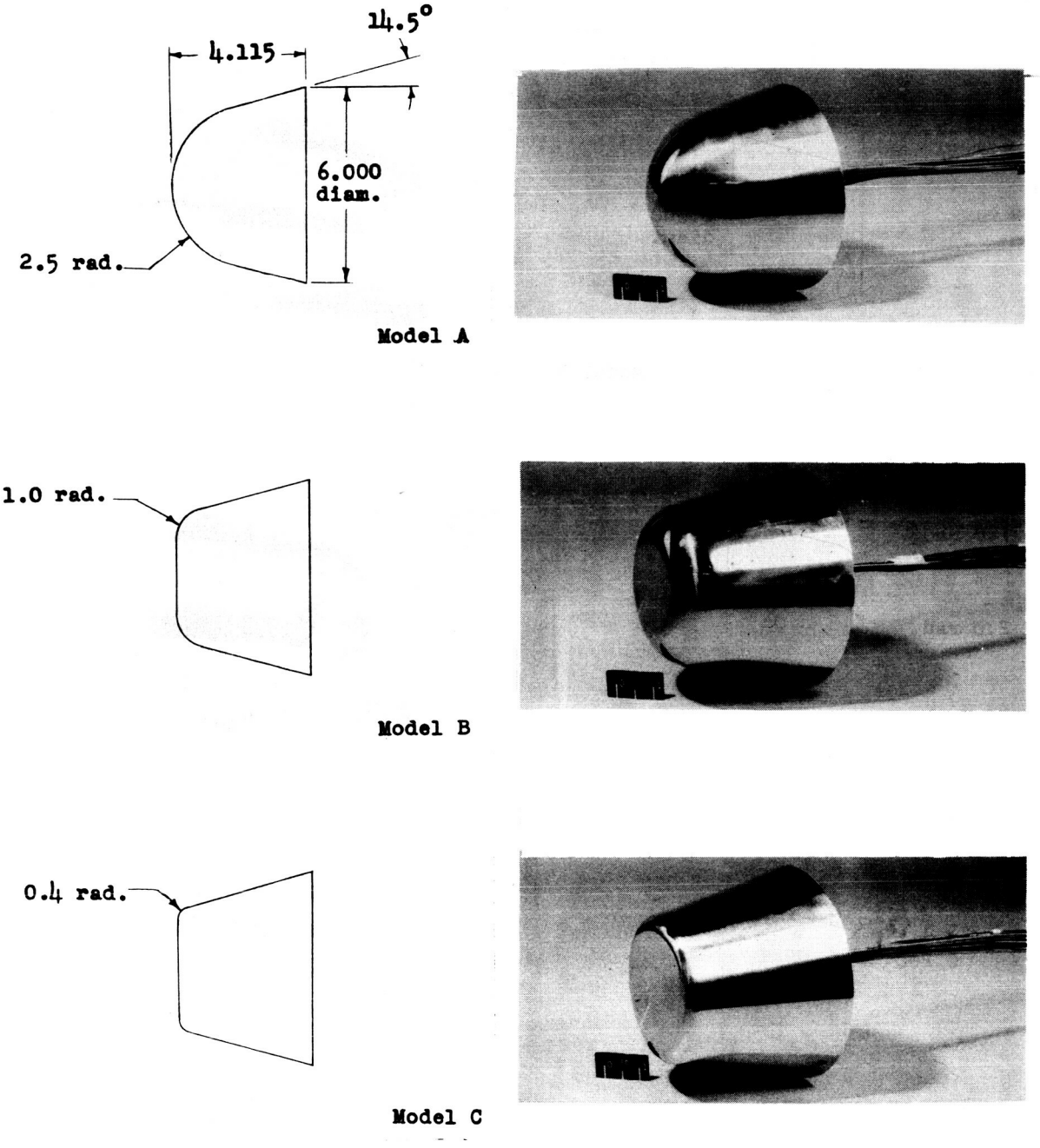

(a) Models A, B, and C. L-57-175

Figure 1.- Drawings and photographs of the six blunt-nose models. All dimensions are in inches.

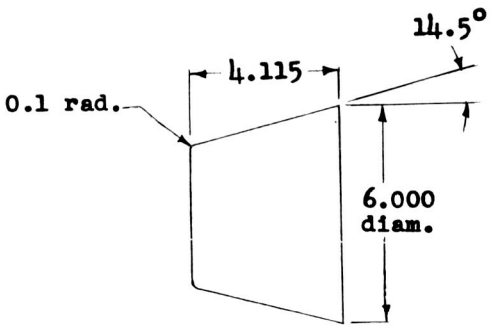

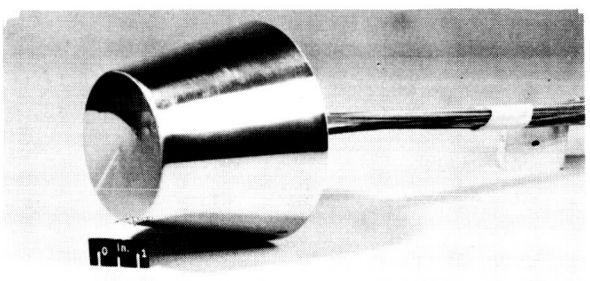

Model D

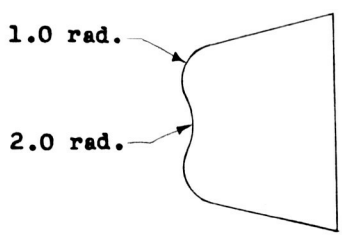

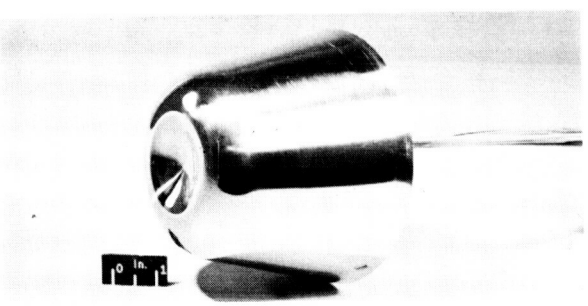

Model E

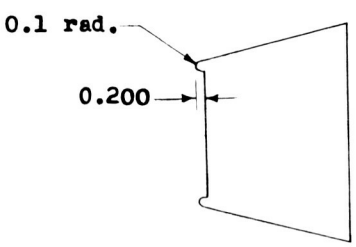

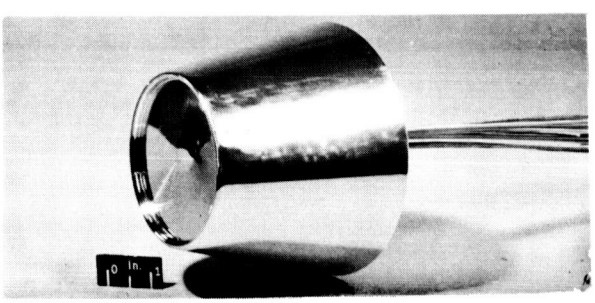

Model F

(b) Models D, E, and F. L-57-176

Figure 1.- Concluded.

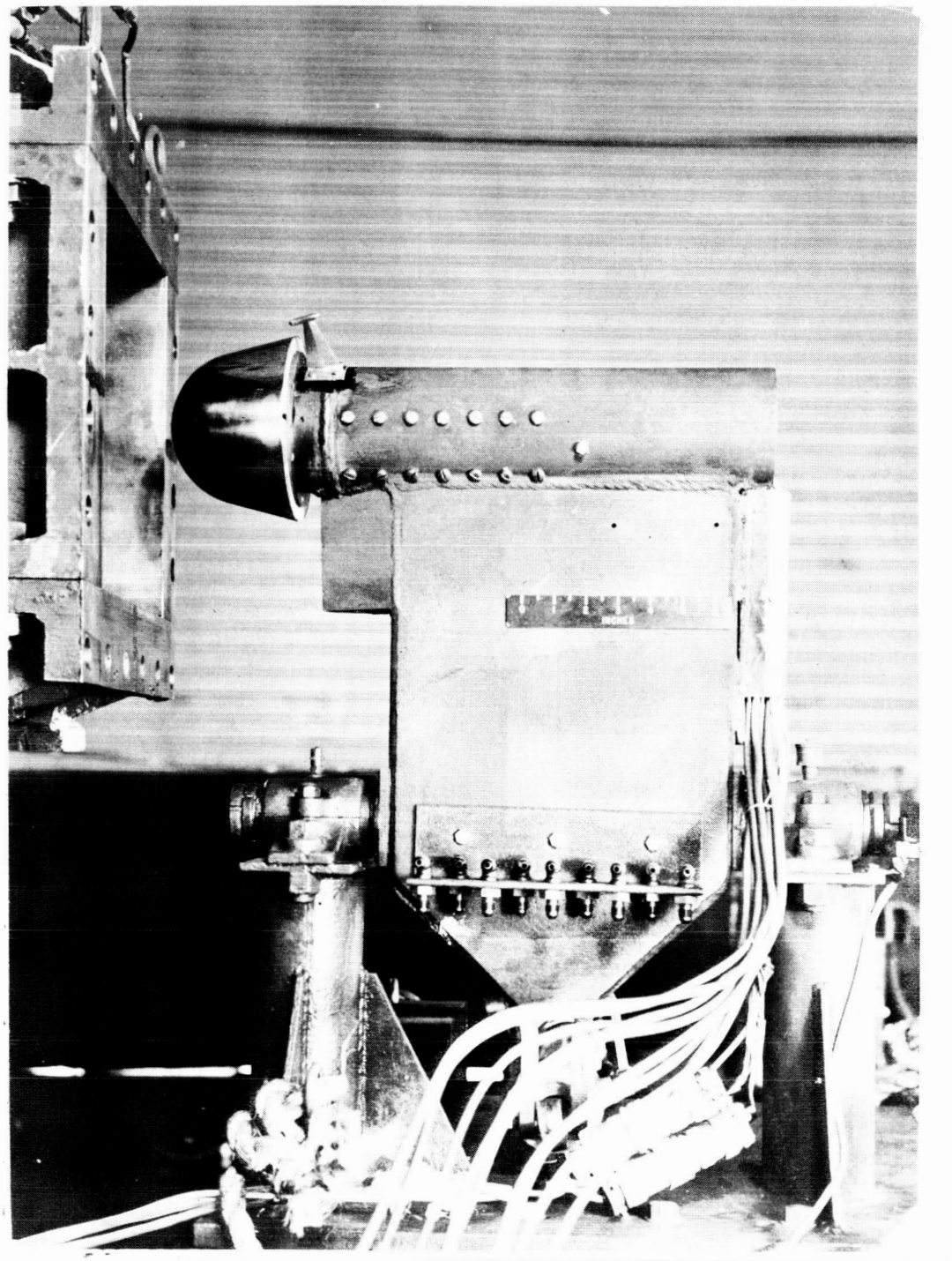

L-95108

Figure 2.- Photograph of model A mounted at the exit of the 12- by 12-inch nozzle in the preflight-jet facility.

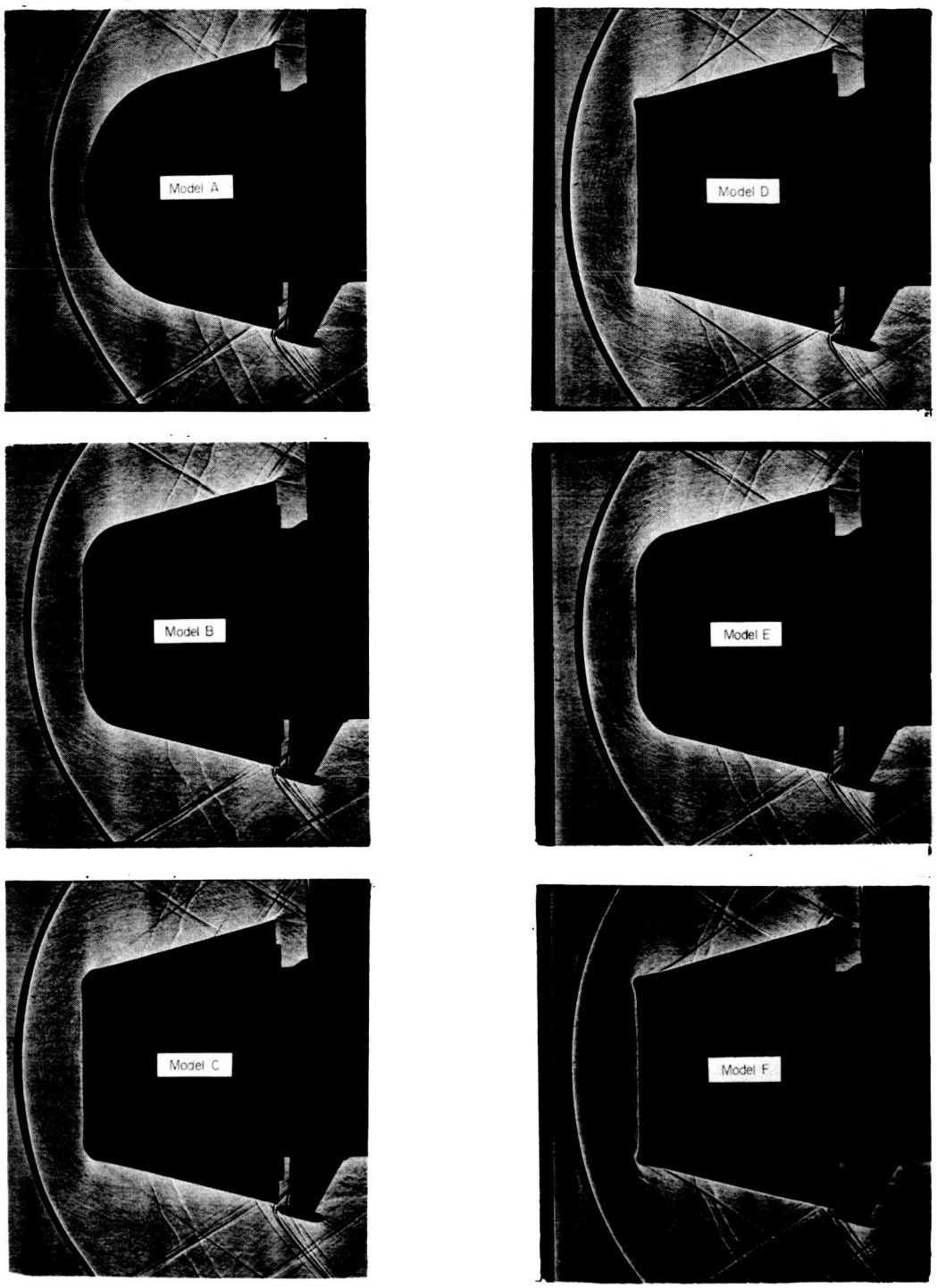

L-57-177

Figure 3.- Shadowgraphs of the models in the free jet at an angle of attack of 0°.

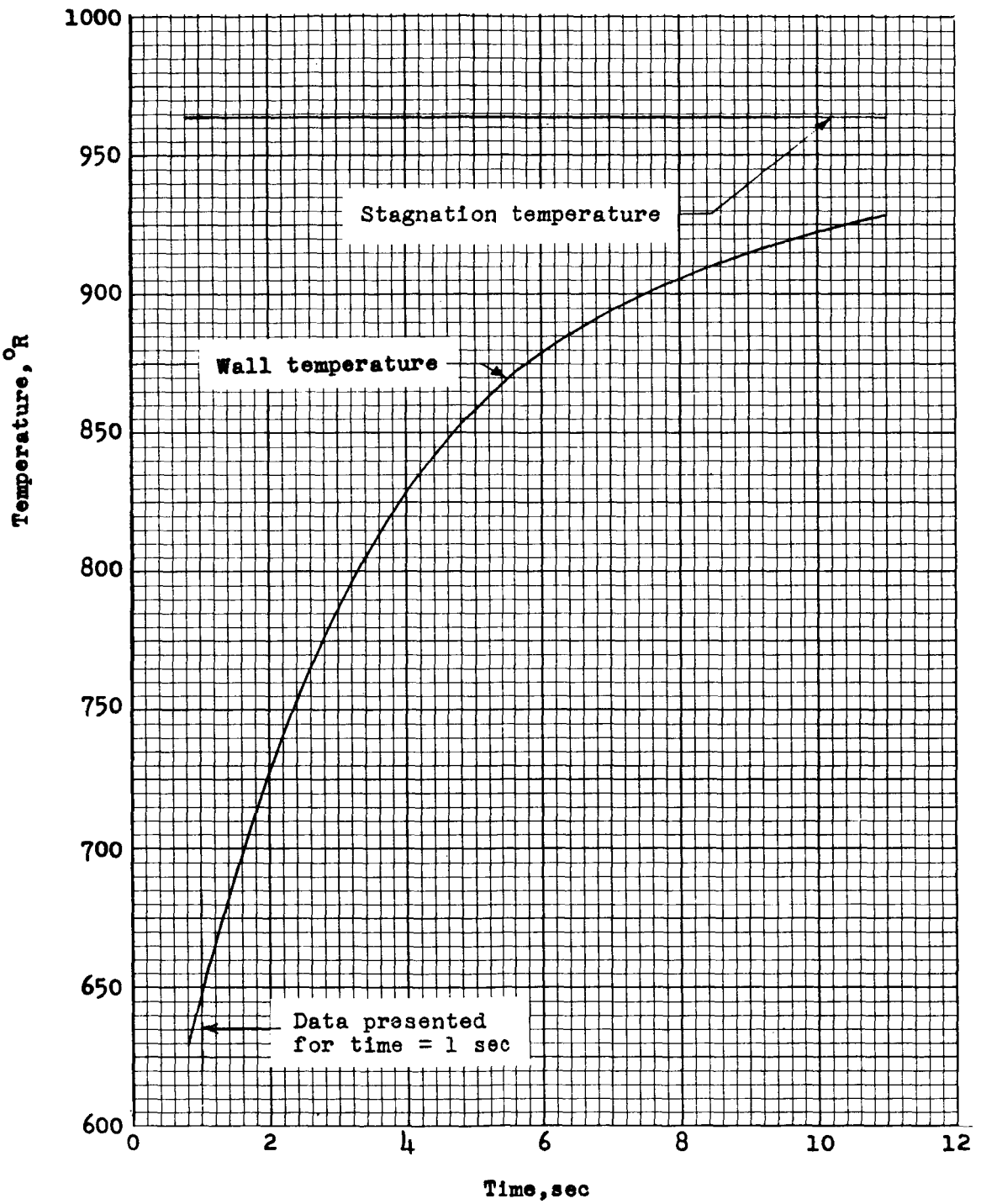

Figure 4.- Typical temperature-time curves for wall temperature and free-stream stagnation temperature.

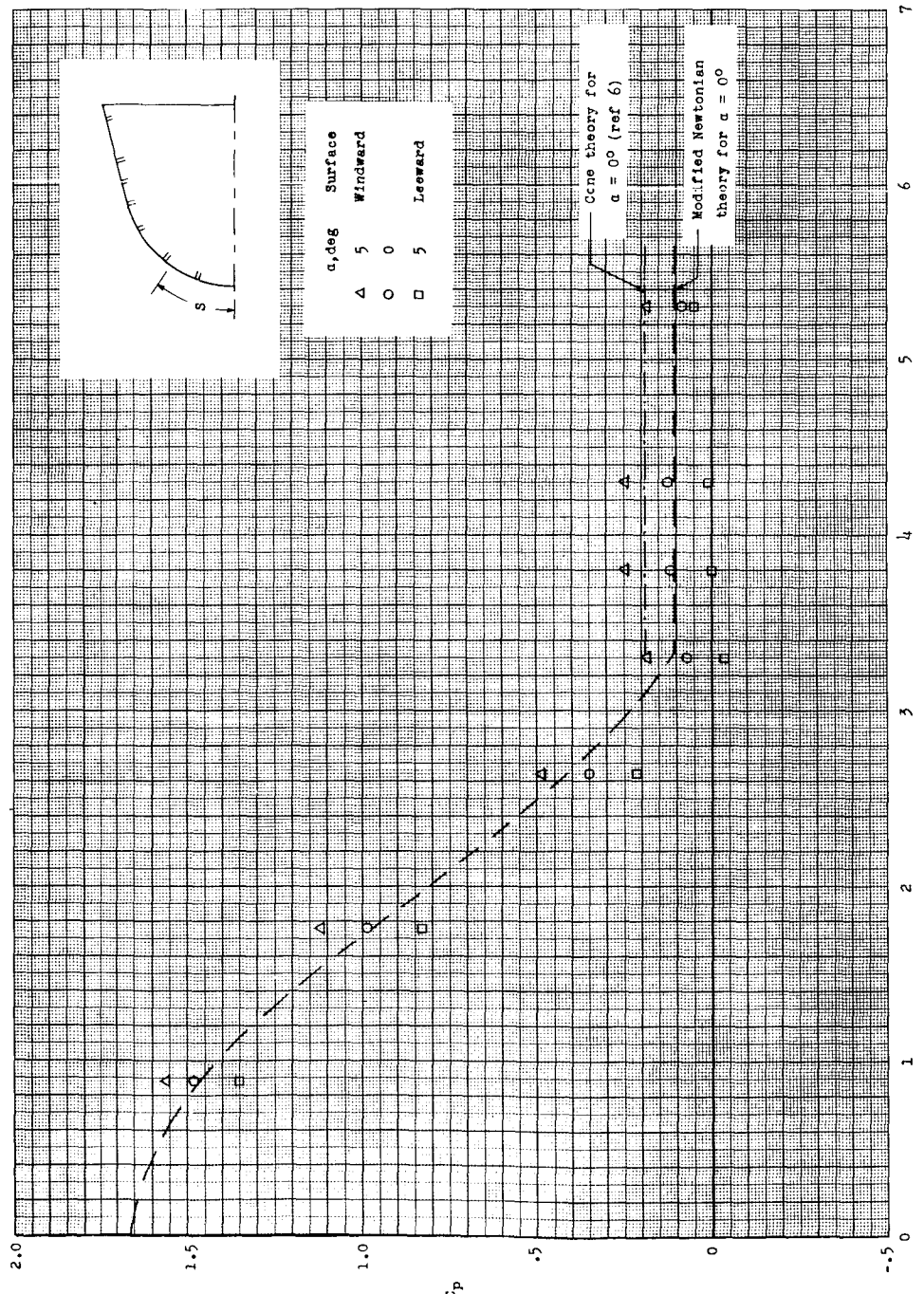

(a) Model A.

Figure 5.- Pressure distributions for the six models.

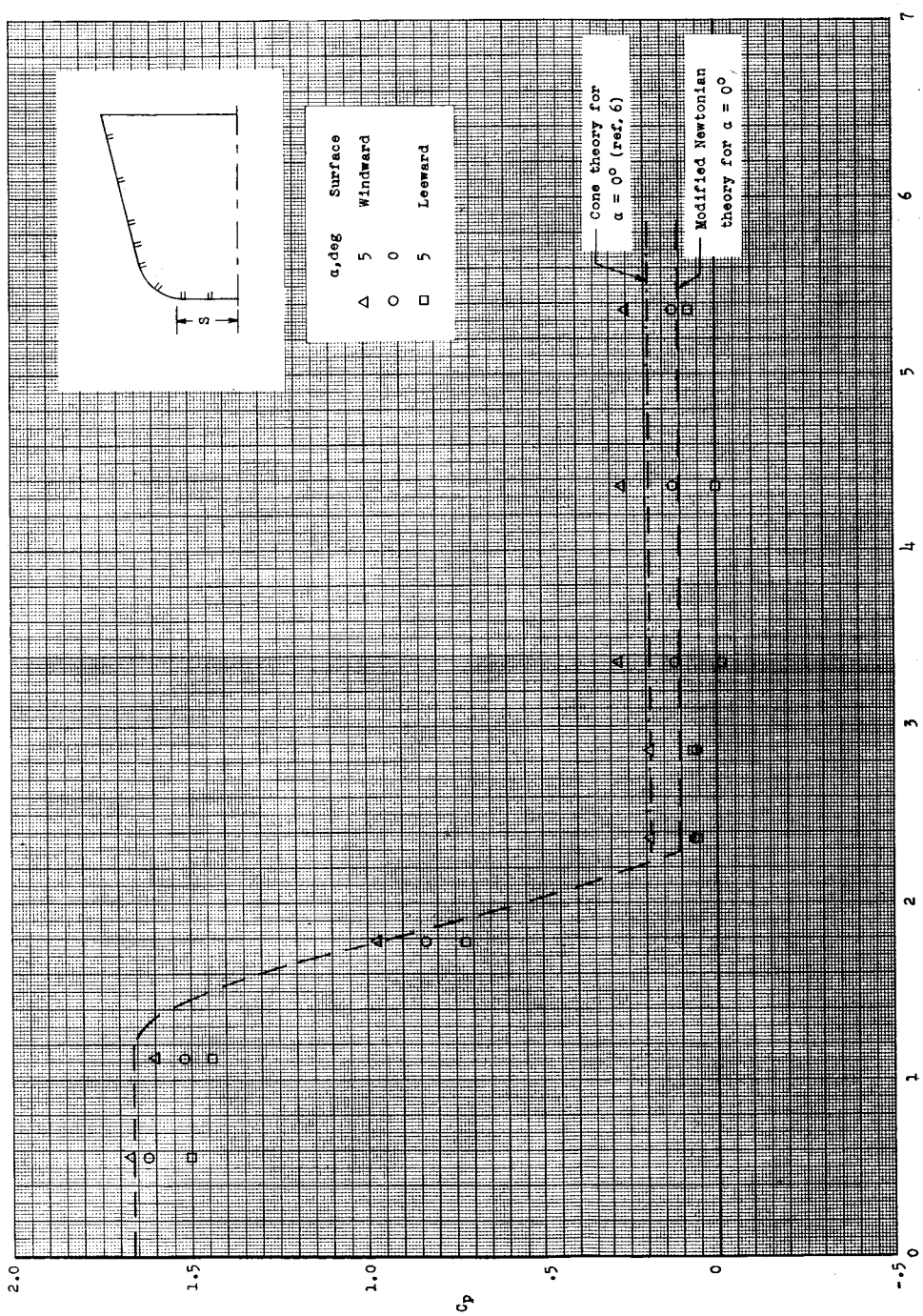

(b) Model B.

Figure 5.- Continued.

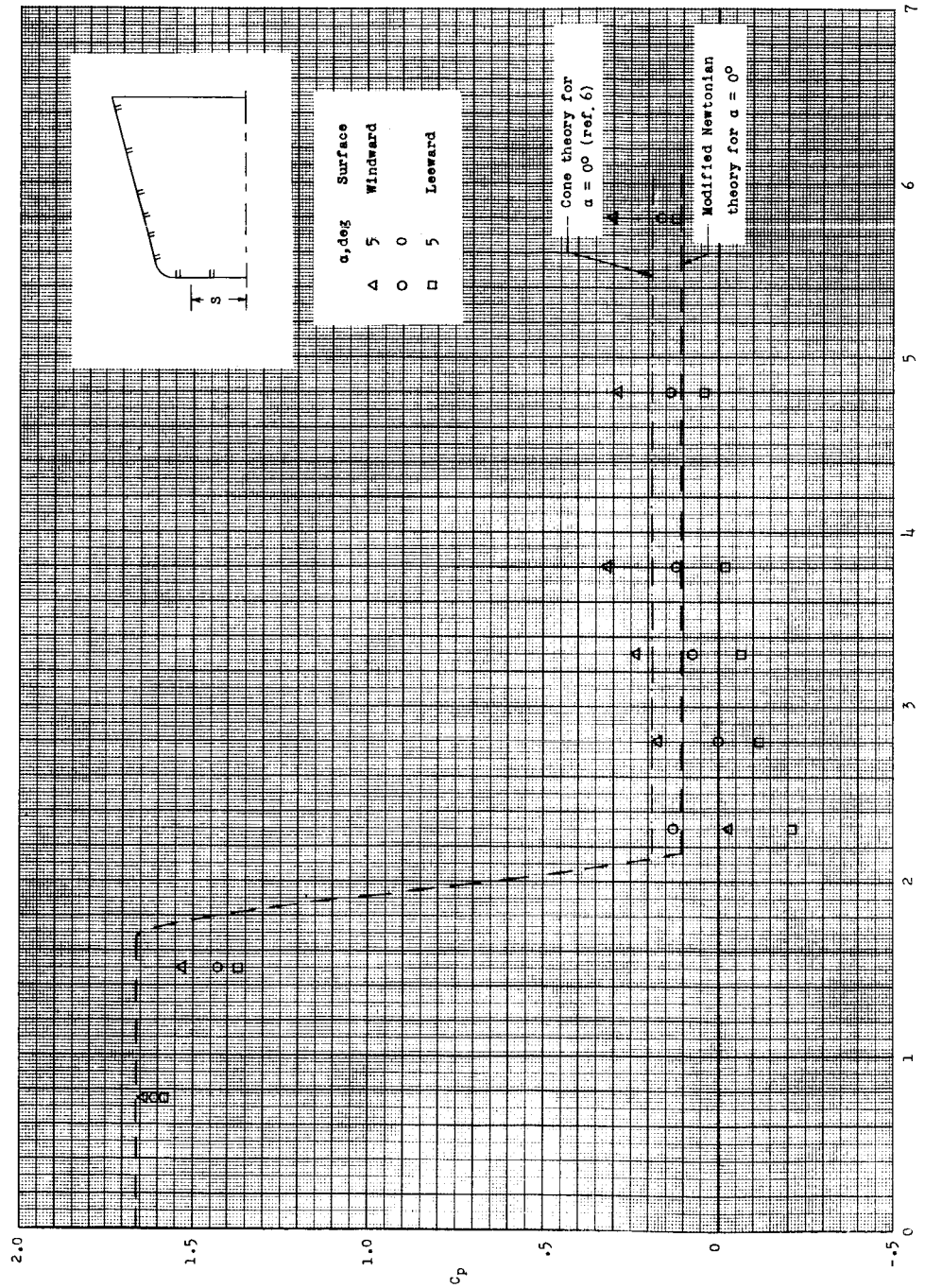

(c) Model C.

Figure 5.- Continued.

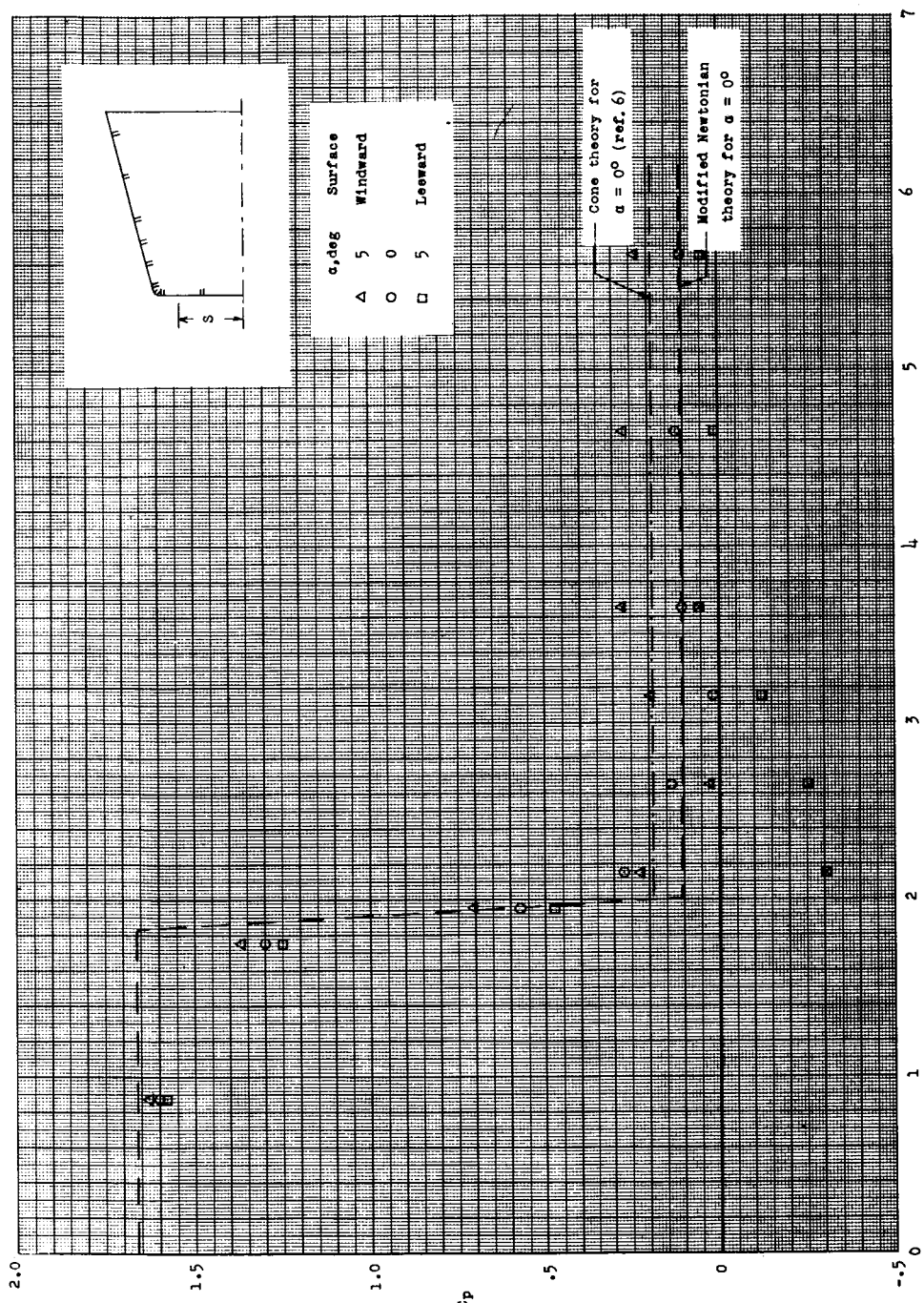

(a) Model D.

Figure 5.- Continued.

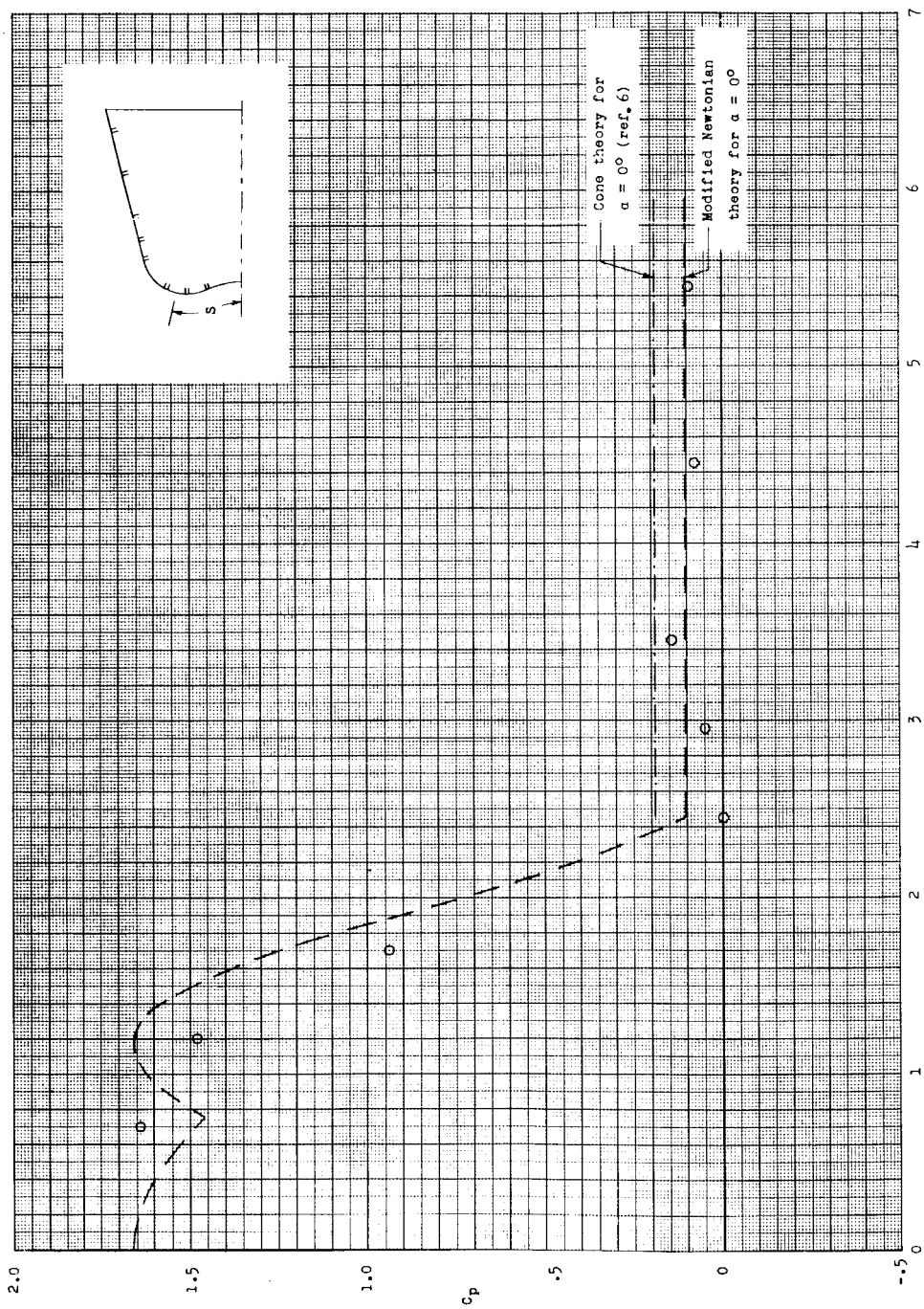

(e) Model E.

Figure 5.- Continued.

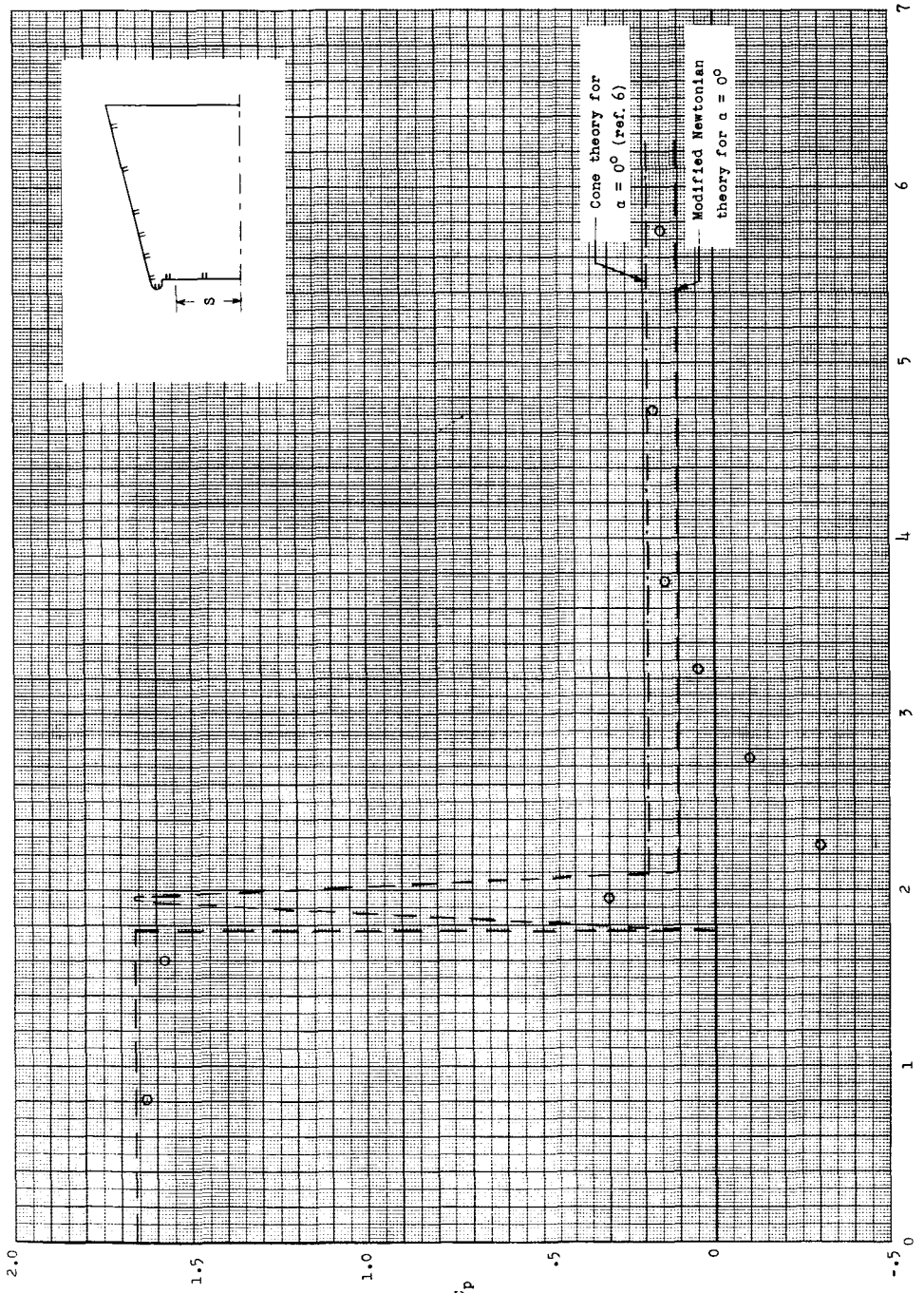

(f) Model F.

Figure 5.- Concluded.

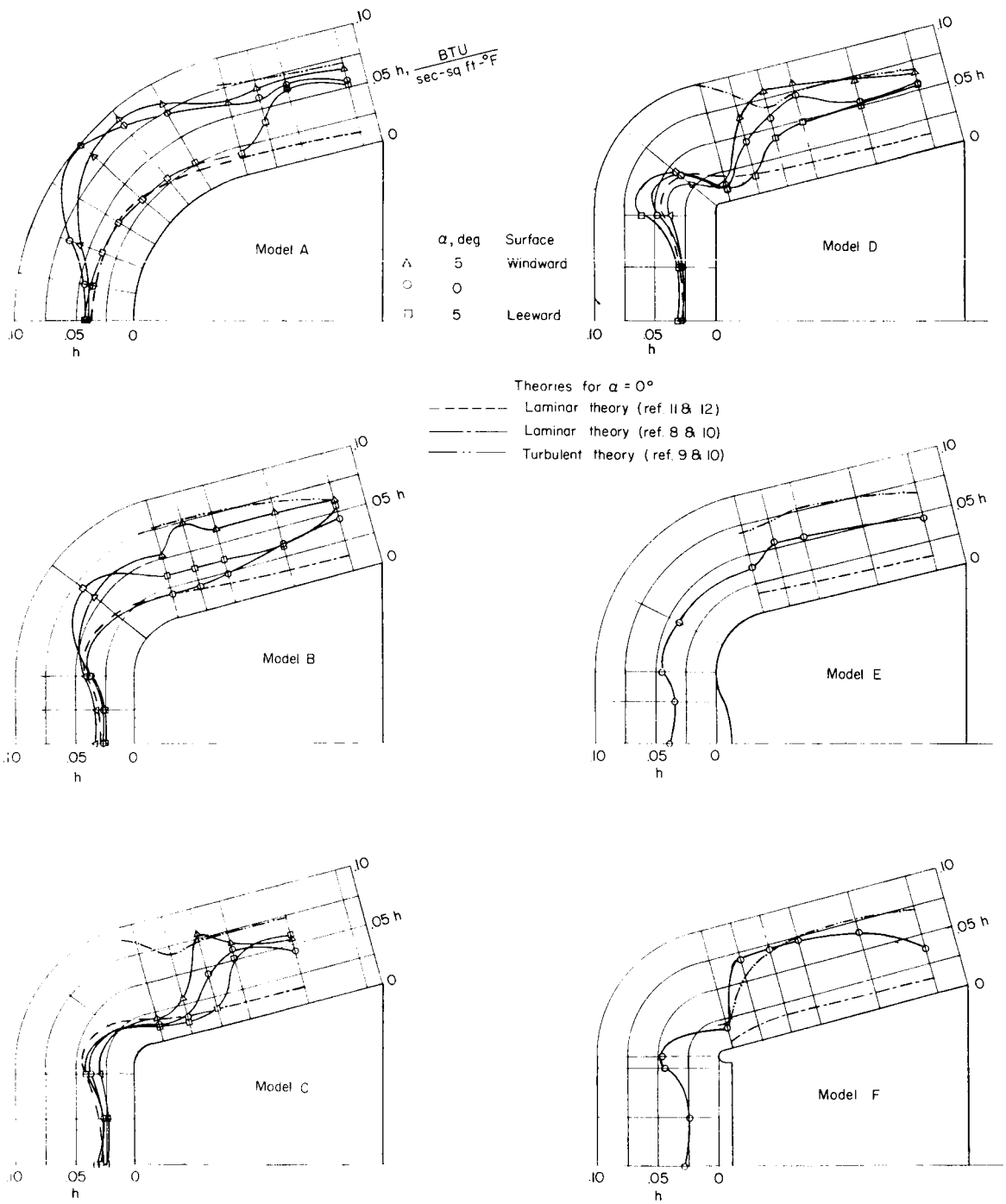

Figure 6.- Heat-transfer coefficients for the six models.